

0017-9310(94)00220-7

Prandtl number effect on offset fin heat exchanger performance: experimental results

SEN HU and KEITH E. HEROLD†

Center for Environmental Energy Engineering, University of Maryland, College Park, MD 20742, U.S.A.

(Received 6 August 1993 and in final form 7 July 1994)

Abstract—This paper describes an experimental apparatus to study heat transfer and pressure drop of liquid-cooled offset fin compact heat exchangers (cold plates). Liquid coolants used in the test are water and polyalphaolefin, for which the Prandtl number ranges from 3 to 150. From the comparison with previous air-cooled models, the liquid-cooled experimental data show that the Prandtl number has a large effect on the Nusselt number of the offset fin geometry. A numerical heat transfer analysis was performed to investigate the surface temperature distribution and uniformity of heat flux in the cold plates. The results demonstrate good agreement with experimental surface temperature measurements. The model results were used to guide data reduction procedures. In particular, significant end effects are predicted. Through experience with the heat transfer model, these end effects were isolated.

INTRODUCTION AND BACKGROUND

Compact heat exchangers are widely used for electronic cooling in many industries, including aerospace and automotive, because of light weight and small size. A typical compact heat exchanger employs fins as extended heat transfer surface. The fin geometry can be plain fins, offset fins, perforated fins, wavy fins, pin fins and louvered fins as described by Manglik and Bergles [1]. An experimental study of the performance of symmetrical offset fins with liquid coolants is described in this paper.

Kays and London [2] carried out early experimental investigations on the offset fin geometry. Later Kays [3], Briggs and London [4], London and Shah [5], Mochizuki and Yagi [6], and Mochizuki *et al.* [7] extended the experimental research on similar geometries. Sparrow and Hajiloo [8] used mass transfer to simulate heat transfer on scaled-up offset fin arrays. Joshi and Webb [9] performed pressure drop tests on eight scaled-up offset fin geometries. These experimental results provided the basis for later theoretical and numerical investigations. Many empirical correlations have been proposed based on the experimental data. Wieting [10] built an empirical correlation of Colburn factor j and Fanning friction factor f , based on existing experimental data. Kays and London [11] compiled the experimental results for 21 offset fin arrays. A comprehensive review of the experimental research on the offset fin geometry is found in Manglik and Bergles [1].

All the studies mentioned above employ air as the

coolant. In some applications liquids are preferred to air as cooling fluids because of better heat transfer properties. This provided the motivation to investigate whether the models for air can predict the liquid-cooled heat transfer characteristics.

Compared to the research using air, very little experimental work has been published using liquid coolants in offset fin heat exchangers. The following studies represent all such work known to the authors. Robertson [12] tested the heat transfer performance of an offset fin cold plate using liquid nitrogen at 80 K with Prandtl number about 24. Brinkmann *et al.* [13] conducted experiments on two offset fin arrays using water and dielectric fluorocarbon (FC-77), for which the Prandtl number ranges from 6 to 25. Each fin array had only four rows of offset fins and, therefore, the entry length effects on the fin array are large. Hou [14] performed an experimental study on one offset fin array, using water and ethylene glycol, for which the Prandtl number ranges from 6 to 40. In the Hou study, there are 80 rows of fins in the fin array and thus the configuration is similar to the geometries considered in the present study. Marr [15] proposed that heat transfer to a single-phase liquid can be predicted by modifying the results of air-cooled correlations by the factor $(Pr_l/Pr_s)^{0.25}$, where Pr_l and Pr_s are the Prandtl numbers at the liquid temperature and surface temperature. Unfortunately, Marr provided no comparisons between the model and experimental data. LeVasseur [16] measured the maximum surface temperatures on a flow-through SEM-E electronic module as a function of water flow rate. Prandtl number effects on heat exchanger performance were found in these investigations, but the limited nature of the

†Author to whom correspondence should be addressed.

NOMENCLATURE

A	total heat transfer area in a unit	Re^P	Reynolds number of parallel plates channel, uD_h^P/ν
A_2	heated area at bottom in a unit, $2l(s+t)$	Re	Reynolds number based on offset fin, uD_h/ν
A_c	front area of a unit, sh	s	fin spacing distance
A_F	fin area in a unit	t	fin thickness
D_h	hydraulic diameter of offset strip fin	T_s	surface temperature
D_h^P	hydraulic diameter of parallel plates channel, $2h$	T_f	fluid temperature
f	average Fanning friction factor in offset fin	u	fluid velocity in the area sh
h	fin height	U	average overall heat transfer coefficient in a unit
h_0	average heat transfer coefficient of fin array	$U_{1,x}$	local unit average overall heat transfer coefficient of section I
$h_{0,x}$	local unit average heat transfer coefficient of a unit	$U_{2,x}$	local unit average overall heat transfer coefficient of section II
j	Colburn factor, $Nu_0/(Re Pr^{1/3})$	$U_{3,x}$	local unit average overall heat transfer coefficient of section III
k	thermal conductivity of fluid	v	fluid velocity in the area $(s-t)h$
k_A	thermal conductivity of aluminum plate	x	distance from beginning of the duct in x -direction
l	fin length	x^{P*}	nondimensional thermal entry length of parallel plates.
L	fin array length		
L'	length of a unit cell, $2l$		
Nu_0	average overall Nusselt number in a unit, $h_0 D_h/k$		
Nu_x^P	local Nusselt number of parallel plates, $U_{i,x} D_h^P/k$		
ΔP_L	pressure drop of the fin array with length of L		
Pr	Prandtl number of fluid		
Pr_1	Prandtl number at fluid temperature		
Pr_s	Prandtl number at surface temperature		
q	heating flux		

Greek symbols

α	aspect ratio, s/h
δ	t/l
γ	t/s
η	heat transfer surface efficiency
η_F	fin efficiency
ν	kinematic viscosity of fluid
ρ	density of fluid.

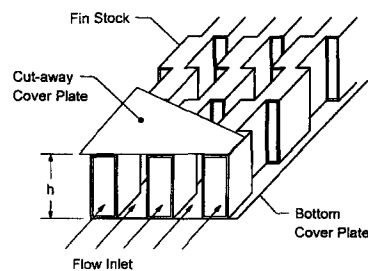
studies did not fully define the Prandtl number effect on offset fin performance. The objectives of the effort described in this paper were to more fully document the Prandtl number effect on offset fin heat transfer.

EXPERIMENTAL FACILITY DESCRIPTION

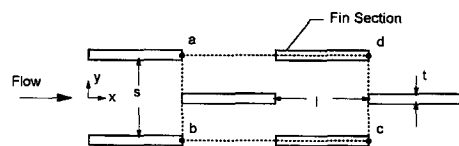
An experimental facility was constructed to conduct heat transfer and pressure drop tests using liquid coolants. The system is designed to provide approximately uniform heat flux on the test section. Heat transfer and pressure drop measurements were performed on seven offset-fin heat exchangers, which are also called cold plates in the following discussion.

Test section

The offset fin geometry, defined in Fig. 1, is vacuum brazed into a cold plate assembly. The cold plates, made from aluminum, were manufactured to our specifications. The fin array is manufactured by cold-chiseling a thin aluminum sheet to a specific fin geometry using rotating toothed dies and was obtained from commercial vendors. Seven different



a. Perspective View



b. Cross Section View at Half Fin Height

Fig. 1. Offset fin geometry.

Table 1. Cold plate fin geometry

Cold plate	Fin thickness, t [mm (in.)]	Fin length, l [mm (in.)]	Fin height, h [mm (in.)]	Fin spacing distance, s [mm (in.)]
1	0.152 (0.006)	3.20 (0.126)	2.39 (0.094)	0.99 (0.039)
2	0.152 (0.006)	3.18 (0.125)	2.34 (0.092)	1.65 (0.065)
3	0.152 (0.006)	6.12 (0.241)	2.26 (0.089)	1.52 (0.060)
4	0.152 (0.006)	3.33 (0.131)	3.84 (0.151)	1.28 (0.050)
5	0.152 (0.006)	3.40 (0.134)	2.36 (0.093)	1.26 (0.049)
6	0.102 (0.004)	3.33 (0.131)	2.36 (0.093)	1.55 (0.061)
7	0.152 (0.006)	3.33 (0.131)	3.84 (0.151)	1.62 (0.064)

fin geometries were used in fabricating the cold plates tested in this effort. The fin geometry parameters, listed in Table 1, were selected to provide a range of fin thickness, fin length, fin height and fin spacing. The cold plate external dimensions are 508×102 mm with height ranging from 7.6 to 9.1 mm.

During the experiment, the cold plate was heated on one side by an electric heater, while all other sides were thermally insulated. The face which contacts the heater is manufactured with flatness of 0.002" TIR (total indicator reading) to provide good contact between the heater and the cold plate. Two measures are taken to reduce the contact thermal resistance between the cold plate and heater assembly. The first is to minimize the gap size. Six C-clamps are used to hold the two plates as close as possible. Wood pads are used between the C-clamps and the cold plate to reduce heat conduction through the C-clamp and to avoid deformation of the cold plate due to the force from the C-clamps. Secondly, a high thermal conductivity paste was used as a filler between the surfaces. The thermal paste is made of silver powder and conductive resins with a thermal conductivity of $4.5 \text{ W m}^{-1} \text{ K}^{-1}$, according to the manufacturer. The electric heater (main heater), designed to provide uniform heat flux over the heated surface, provided heat flux up to 7.5 W cm^{-2} (total power up to 1750 W).

Test loop

The test loop, shown schematically in Fig. 2, is a recirculating liquid loop. A shell and tube heat exchanger is employed as the system heat rejection to a glycol chiller loop. Filters, with pore size of $60 \mu\text{m}$, are used in the system to eliminate particles in the flow.

Coolant fluids used in the tests are water and PAO (polyalphaolefin), which is a low-viscosity oil. The Prandtl number for the tests ranged from 3 to 150. The inlet fluid temperatures were selected as 10, 20 and 60°C , which influences the Prandtl number. Fluid flow rates and heater power inputs were varied over the full range available from the facility (coolant flow rate: $3\text{--}11 \text{ l min}^{-1}$; heater power: $400\text{--}1750 \text{ W}$). Due to dissolved salts existing in normal tap water, significant scale buildup on the fin structure was experienced in initial testing. Scale formation causes a sig-

nificant increase of pressure drop and decrease of Nusselt number in the cold plate. The scaling was apparently augmented by an electrochemical cell formed between the copper tube and aluminum cold plate, which caused deposits on the aluminum. To prevent scale formation, two methods were used: (1) plastic tube-fittings were installed between the copper tube and aluminum cold plate to eliminate the electrochemical cell; and (2) deionized water with low salt concentration was used. These measures completely eliminated the scale problems experienced in initial testing.

The cold plate assembly and connecting lines were insulated to minimize temperature gradients due to heat loss. The energy balance on the cold plate and heater assembly showed a heat loss of up to 8% of the power input at high-temperature conditions. This loss did not cause a problem since the data analysis was based on the energy added to the liquid.

The inlet fluid temperature to the test section is controlled by a trim heater connected to a PID temperature controller. This system provided a stable inlet temperature. Referring to Fig. 2, the two-tank design allows calibration of the turbine flow meters. Calibration curves for both flow meters were obtained with each fluid and over the complete range of experimental temperatures.

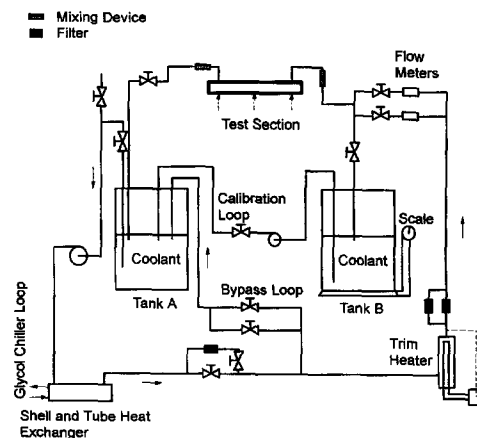


Fig. 2. Liquid test loop.

Instrumentation

Cold plate surface temperatures are measured by 14 copper–constantan thermocouples (type T) with a wire diameter of 0.076 mm mounted between the heater assembly and the cold plate. Ten grooves (0.16 × 0.16 mm) were machined on the heater assembly surface to carry the thermocouple lead wires. Thermocouples arranged along the center line measured the surface temperature distribution in the flow direction. The inlet and outlet fluid temperatures are measured by thermocouples before and after the test section. Fluid mixing devices were used upstream of the measurement locations to obtain bulk fluid temperatures. An ice bath is used as the reference for all the temperature measurements. The thermocouples were calibrated individually against a platinum resistance thermometer with an absolute accuracy of better than 0.01 K. Temperature measurement accuracy is estimated to be ±0.1°C.

The power of the main heater was measured by a power transducer with a stated accuracy of ±5 W. A differential pressure transducer was used to measure the pressure difference through the fin array. The differential pressure transducer was calibrated with a manometer using mercury and water for different ranges. The pressure transducer has a stated accuracy of ±10 Pa. The liquid flow rate was measured by one of two turbine flow meters for different ranges. Flow meters were calibrated by use of the calibration loop discussed previously. The flow rate measurement system with the large flow meter has a range of 3–43 l min⁻¹ and an accuracy of ±0.067 l min⁻¹. The flow rate measurement system with the small flow meter covers the range 0.7–2.9 l min⁻¹ with an accuracy of ±0.016 l min⁻¹.

THERMAL SPREADING AND END EFFECTS

The experiment was designed to apply a constant heat flux to the cold plate. Thus, the surface temperatures increase in the flow direction, which causes minor heat conduction in the heater assembly and cold plate. This effect is called thermal spreading in the following discussion. Conduction effects also exist in the unheated end sections, which are termed the end effects. End effects and thermal spreading in a similar geometry are discussed by Philips [17], who applied constant heat flux on liquid cooled microchannel heat sinks. To estimate these effects in the current study, a numerical heat transfer model called the spreading model was created to predict system temperatures.

The spreading model is based on a two-dimensional cross-section of the geometry of a cold plate, as shown in Fig. 3. The finite difference model is designed to calculate the temperature distribution and heat transfer in the section *a–b–c–d*, which models the aluminum cover plate. Surface *b'–c'* is heated by the main heater. Surfaces *a–b*, *c–d*, *b–b'* and *c–c'* are insulated.

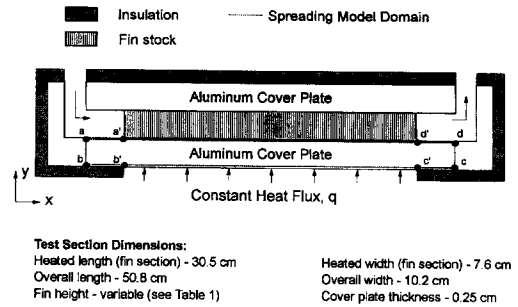


Fig. 3. Test section geometry and geometry used in thermal spreading model.

Equations and boundary conditions

Two-dimensional conduction in the plate is modeled assuming constant thermal conductivity. For this situation, the temperature field obeys the Laplace equation

$$\frac{\partial^2 T}{\partial x^2} + \frac{\partial^2 T}{\partial y^2} = 0 \quad (1)$$

which was discretized using a constant volume formulation. Referring to Fig. 3, all boundary conditions except surface *a–d* were constant heat flux with the flux on the insulated boundaries set to zero. Surface *a–a'* experiences convective heat transfer, which is modeled as developing flow between two infinite parallel plates [18]. The local overall heat transfer coefficient on the surface *a–a'*, $U_{1,x}$, is

$$U_{1,x} = \frac{Nu_x^p k}{D_h^p} \quad (2)$$

The local overall heat transfer coefficient on surface *d–d'*, $U_{3,x}$, is calculated in the same manner as $U_{1,x}$ assuming laminar, developing heat transfer. The total heat transfer from these end sections is a small fraction (less than 3.0%) of the total heat transfer in the cold plate. Thus, an approximate model for these sections is adequate for the purpose of calculating the overall heat transfer.

Surface *a'–d'* represents the fin array. The extended surface is modeled as an effective Nusselt number. The Nusselt number is influenced significantly by thermal development in the fin array. A model for the effective, local, fin-average heat transfer coefficient of the offset fin array, $h_{0,x}$, is given in a companion paper [19, 20]. The local fin-average overall convective heat transfer coefficient on the finned surface *a'–d'*, $U_{2,x}$, has the form

$$U_{2,x} = \frac{h_{0,x} A \eta}{A_2} \quad (3)$$

The heat transfer surface efficiency η is a function of the fin efficiency, η_F , discussed in a later section.

Numerical model results and discussions

The difference equations consist of a coupled set of linear algebraic equations in the unknown tempera-

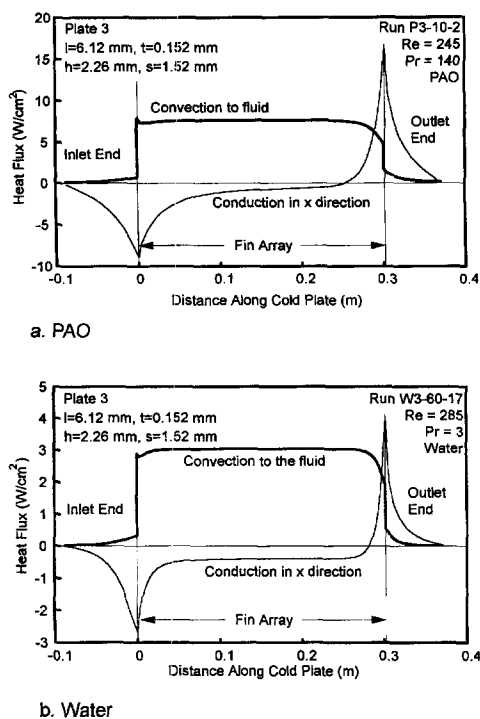


Fig. 4. Calculated heat flux in the offset fin cold plate.

tures. The Gauss–Seidel method was used to solve the equations iteratively. Program inputs include coolant flow rate, heating power and inlet fluid temperature. Data from an experimental run were input to the model in order to compare the model predictions with experimental surface temperatures. The average fluid temperature is used to calculate the fluid thermal properties. The model was run for each of the experimental runs. In the final version discussed here, the effective heat transfer coefficients for the offset fin array were obtained from our experimental data. Therefore, the numerical model predicts the surface temperature distribution quite well. The real value of the model is that it reveals the relative importance of the heat transfer mechanisms in an offset fin cold plate. In addition, the model was used to help interpret the experimental surface temperature data.

The conductive and convective heat transfer are calculated by the numerical model. The results presented here are representative of the predictions of the model. Two experimental cases with similar Reynolds number are selected to show the Prandtl number effect on the distributions of heat flux and surface temperature. Figure 4(a) and (b) shows the heat flux distribution vs plate length in the flow direction for plate 3. Figure 4(a) represents the case with a Reynolds number of 245 and Prandtl number of 140. Figure 4(b) represents the case with Reynolds number of 285 and Prandtl number of 3. The thin line represents the conductive heat flux in the x -direction and the thick line is the convective heat flux to the fluid. It should be noted that the two fluxes are based on different

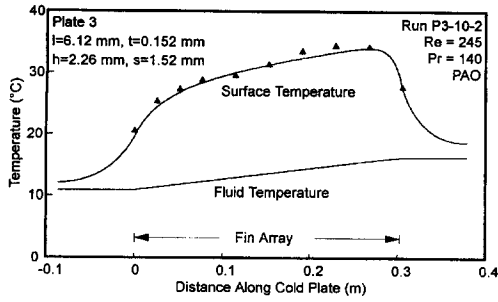
areas and thus cannot be compared directly. It can be seen that conduction effects are relatively large at both ends of the heated section (which corresponds to the fin array), which is due to the large temperature gradients existing between the heated and unheated regions. The conduction at both ends influences the convection through the surface temperatures, causing non-uniform heat flux near the ends. The results indicate that end effects are significant for approx. 0.03 m at the inlet and 0.07 m before the exit of the fin array.

Thermal spreading (i.e. conduction) is present in the finned region, but is not particularly important. Compared to the end effects, the effect of thermal spreading in the central section is small. At the center of the cold plate, the conduction heat transfer rate is only 0.2% of the total power input.

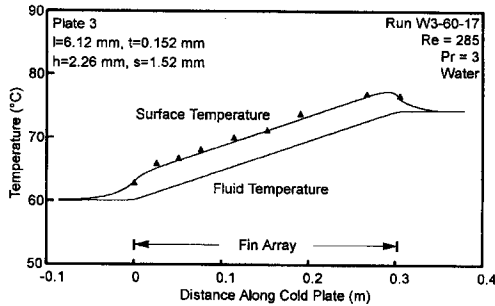
The shape of the convective curve at the inlet end is due to two factors. The initial peak and following drop off at the beginning of the fin array is due to the shape of the heat transfer coefficient as the flow approaches a periodic fully developed regime. The minimum in the curve is due to conduction (end effect) transferring heat to the unheated inlet region, which decreases the surface temperatures and reduces the convective heat transfer. At the exit end of the fin array, the convective heat flux drops, which is also due to the end effect where conduction to the unheated exit region is important. Sufficiently far from both ends, the calculations indicate an essentially constant convective heat flux over the central section of the fin array.

Figure 4(a) and (b) shows similar convective heat flux distributions along the fin array. These results support the assumption of constant heat flux used in our data analysis. The results of the model were used as a guide in isolating end effects from the data. As was already noted, the convection and conduction heat fluxes are based on different heat transfer areas. The conduction heat transfer area is the cross-section area of the cold plate, which is much smaller than the convection area. Thus, the total convection heat transfer is much larger than the conduction heat transfer in the x -direction. For example, for the case shown in Fig. 4(a), the conduction heat transfer rate at the center of the plate is 3 W, while the convection heat transfer rate is 1500 W. However, at the outlet end, the conduction rises to a peak value of 33 W.

Comparisons between the numerical model predictions and experimental data for the surface temperatures for the same two cases are shown in Fig. 5(a) and (b). It can be seen that the experimental surface temperatures exhibit the same trend as the model results. The lower surface temperature at the beginning of the fin array is caused by end effects due to conduction, and by the effect of developing convective heat transfer. It can be seen that the surface temperatures in the inlet and exit regions are higher than the fluid temperature, which is due to conduction from the heated area to the unheated area. This heat is then transferred to the fluid by convection. Due to



a. PAO



b. Water

Fig. 5. Cold plate temperatures from numerical model and experiment.

the relatively low Nusselt number in the entrance and exit un-finned sections, the fluid temperature does not change significantly in these sections. In the heated section, the fluid closely follows a linear temperature distribution in the flow direction consistent with the approximately uniform heat flux. A linear fluid temperature distribution is assumed in the experimental data reduction.

Figure 5(a) represents the case with Reynolds number of 245 and Prandtl number of 140. For these Reynolds and Prandtl numbers, thermal development is important in the heat transfer in the fin array. In the entry region of the fin array, the convective heat transfer coefficient is high due to thermal development effects. In Fig. 5(a), it can be seen that the difference between the surface and fluid temperatures in the developing region is smaller than that near the exit. Figure 5(b) represents the case with Reynolds number of 285 and Prandtl number of 3. Figure 5(b) shows that the thermal development effect is relatively small. For this case, the temperature difference between the surface and fluid is approximately constant over the length of the fin array.

DATA REDUCTION

The data reduction procedure is based on the offset fin geometry in Fig. 1. With one unit chosen as a - b - c - d , the entire fin array can be considered as consisting of many such units. Each unit has the same geometry and is assumed to have the same convective heat flux. The hydraulic diameter is defined as [11]

$$D_h = \frac{2shl}{sl + hl + th} \quad (4)$$

The Reynolds number, Re , is evaluated based on the average flow velocity, u , over the minimum flow area A_c .

Heat transfer data

It should be realized that in the inlet section the cell-averaged local heat transfer coefficient changes along the length in the flow direction. As the flow approaches a periodic fully developed regime, the average heat transfer coefficient approaches a constant value. From measured data, the obtained heat transfer coefficient, h_0 , is the average value over a section of fin array. The analysis is based on a multiple of units such as a - b - c - d in Fig. 1, where the thermal resistance of the unit can be written as

$$\frac{1}{UA} = \frac{b}{A_2 k_A} + \frac{1}{A\eta h_0} \quad (5)$$

In equation (5), the term on the left-hand side represents the total thermal resistance between the heated surface and the bulk fluid, where U is the average overall heat transfer coefficient. On the right-hand side, the first term is the thermal resistance of the aluminum cover plate with thickness b , where k_A is the thermal conductivity of aluminum. The second term is the thermal resistance associated with convection from the offset fins, where η is the heat transfer surface efficiency. Different from an air-cooled application, the resistance of the aluminum cover plate cannot be ignored, since the liquid coolants have significantly higher heat transfer coefficients. For example, when water is used as the coolant, the thermal resistance of the cover plate contributes up to 15% of the total thermal resistance. From equation (5), the unit average heat transfer coefficient, h_0 , has the form

$$h_0 = \frac{1}{\eta} \frac{1}{(1/U) - (bA/k_A A_2)} \quad (6)$$

The average overall heat transfer coefficient, U , is calculated from the data according to

$$U = \frac{Q}{\Delta T_{lm} A} \quad (7)$$

where ΔT_{lm} is the log mean temperature difference between the heated surface and the fluid defined as

$$\Delta T_{lm} = \frac{(T_{s1} - T_{f1}) - (T_{s2} - T_{f2})}{\ln(T_{s1} - T_{f1}) - \ln(T_{s2} - T_{f2})} \quad (8)$$

where points 1 and 2 define the region sufficiently far from both ends as to isolate end effects. The surface temperatures of points 1 and 2 are represented by T_{s1} and T_{s2} . The fluid temperatures along the fin array are calculated based on an assumed linear profile and the measured inlet and outlet temperatures. The average overall heat transfer coefficient for that section, U , can be calculated with equation (7). The heat transfer

surface efficiency, η , is related to the fin efficiency according to

$$\eta = 1 - \frac{A_F}{A} (1 - \eta_F). \quad (9)$$

For data reduction purposes, the fin efficiency, η_F , is calculated based on a one-dimensional fin model with an insulated tip. The unheated plate is lumped together with the fin area, resulting in an effective fin height of $(h+s)$. The fin efficiency expression is then

$$\eta_F = \frac{\tanh(m(h+s))}{m(h+s)}. \quad (10)$$

The fin heat transfer area, A_F , which includes the areas of the offset fins and the unheated plate, can be written as

$$A_F = 4(lh + th) + 2ls. \quad (11)$$

From equations (6)–(11), it can be seen that η and h_0 are interdependent. Thus, an iterative calculation is necessary to determine h_0 from the measured data.

The heat transfer performance is evaluated by transforming the average heat transfer coefficient, h_0 , into a Nusselt number, Nu_0 . An alternative dimensionless heat transfer coefficient often used for offset fin studies is the Colburn factor, j , defined as

$$j = \frac{Nu_0}{Re Pr^{1/3}} \quad (12)$$

where fluid properties are calculated at the mean fluid temperature in the cold plate.

Pressure drop data

The pressure drop measured across the cold plate is dominated by the pressure drop across the fin array. The pressure drop can be expressed in terms of the Fanning friction factor, f , defined as

$$f = \frac{\Delta P_L D_h}{2\rho u^2 L} \quad (13)$$

where ΔP_L is the pressure drop of the fin array of length L in the flow direction. In this way, the characteristics of average heat transfer and pressure drop were obtained from the experiments.

Uncertainty analysis

The uncertainty of the reported results is caused by uncertainties in the fin geometry, in the physical properties of the coolants and in the measurement of temperature, pressure and flow rate. By the method described in Kline [21], the following data represent estimated uncertainties of the experimental data: flow rate $\pm 2.3\%$; logarithmic mean temperature difference $\pm 5.8\%$; hydraulic diameter $\pm 2.3\%$; Colburn factor $\pm 6.2\%$; and friction factor $\pm 4.6\%$. Additional uncertainty is introduced in the fin manufacturing step where worn tools can result in significant variations in the burr on the fins.

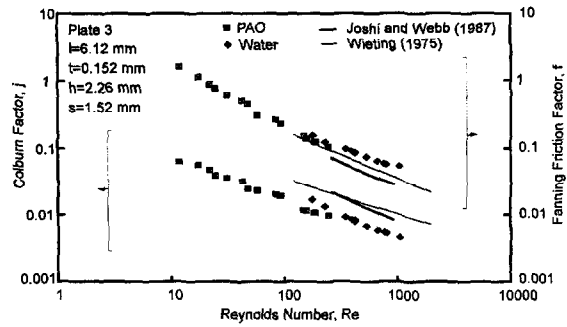


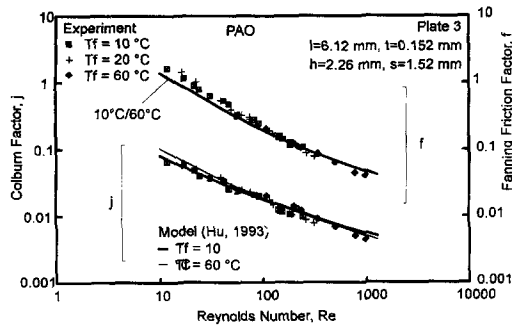
Fig. 6. Comparison of air model and liquid experiments (10°C).

DISCUSSION

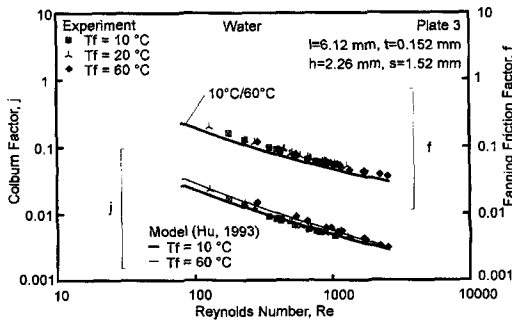
Heat transfer and pressure drop data for liquid-cooled offset fin arrays were obtained from experiments. Figure 6 shows a comparison of experimental data against air correlations from Joshi and Webb [9] and Wieting [10] (note: correlations were modified to use a consistent Reynolds number). Both models are based on experimental data from Kays and London [2], Kays [3] and London and Shah [5], which were obtained from air tests with constant surface temperature. In Fig. 6, the results of both models and experiments are for fluid temperature of 10°C. Comparison between the air models and the experimental results demonstrates that the results for air cannot be accurately applied to liquid applications.

Figure 6 shows that the Colburn factor for liquids is lower than for air. The difference is caused by Prandtl number effects. Because of the definition of the Colburn factor, $j = Nu_0 / (Re Pr^{1/3})$, a large Prandtl number would give a lower j at the same Reynolds and Nusselt number if the Nusselt number were independent of Prandtl number. For the offset fin application, it was found that the Nusselt number increases with Prandtl number but at a rate less than $Pr^{1/3}$. Thus the Colburn factor decreases as Prandtl number increases. But it should be realized that lower j does not necessarily imply a smaller heat transfer coefficient. In Fig. 6, the j of PAO is lower than the j for air, but the heat transfer coefficient of PAO is approximately 5 times larger than that of air.

From the comparison, it can be seen that the Colburn factor for air is approximately twice the Colburn factor for the liquids at the same Reynolds number. The air model overpredicts the heat transfer coefficient for liquids. In cold plate design, this would lead to an underprediction of the heated surface temperature and may cause failure of the components to be cooled. From Fig. 6, it can be seen that the Colburn factor of PAO is very close to the Colburn factor of water. This is partly due to the fact that a higher Prandtl number coolant tends to have a longer developing region. The development length is also proportional to the Reynolds number. Developing heat transfer is more important for PAO than for water. Developing heat transfer



a. PAO Coolant



b. Water Coolant

Fig. 7. Effect of fluid temperature on performance of offset fin cold plate.

means higher heat transfer coefficients, which leads to an increase in j . A detailed discussion of this effect can be found in the companion paper [19].

In Fig. 7, the experimental results with PAO and water at different fluid temperatures are compared with the model proposed in the companion paper [19]. It can be seen that higher-temperature flow with low Reynolds number implies larger j , which is due to the Prandtl number change with fluid temperature. In Fig. 7(a), where PAO is used as the coolant, the Prandtl number ranges from 150 to 40 as temperature ranges from 10 to 60°C. These curves exhibit a significant Prandtl number effect, as shown by the intersection of the j curves for 10 and 60°C. The high Prandtl number fluid has a higher average j at high Reynolds number because of the entry length effects. In Fig. 7(b), where water is used as the coolant, the Prandtl number ranges from 10 to 3 as the temperature ranges from 10 to 60°C. Because of the smaller Prandtl number compared to PAO, no crossover is observed in the j curves. The Colburn factor increases with an increase in Prandtl number. The model results are shown to help understand the mechanism of the Prandtl number effect on the heat transfer performance.

The friction factor includes the surface friction and form drag from the fin geometry, which are both influenced by Reynolds number. For a certain fin geometry and Reynolds number, the friction factor for different Prandtl numbers should be the same. In Fig. 6, the measured friction factor from liquid experiments is found to be higher than that from air models. That is believed to be due to burrs on the fins,

created by the fin manufacturing process. The burrs increase the form drag which increases the overall friction factor. In Fig. 7, the friction factor experimental data have relatively good agreement with the model [19], which considers the effect of burrs by using a form drag coefficient of 1.0.

CONCLUSIONS

A series of heat transfer and pressure drop experiments were performed using liquid coolants in offset fin arrays. The Prandtl number ranged from 3 to 150. The Prandtl number was found to have a significant effect on the Colburn factor, j , of offset fin arrays. Air models overpredict the j factor for liquids. The error implies an underprediction of the surface temperature, which may cause significant design errors. Because the Prandtl number has a significant effect on cold plate performance, it is necessary to build a heat transfer model which covers a large range of Prandtl number. As expected, the Prandtl number was found to have little effect on the Fanning friction factor.

Acknowledgements—The authors would like to express appreciation to Westinghouse Electric Corp. for sponsoring this work. In particular, discussions with Frank Altoz were most helpful.

REFERENCES

1. R. M. Manglik and A. E. Bergles, The thermal-hydraulic design of the rectangular offset-strip-fin compact heat exchanger. In *Compact Heat Exchangers* (Edited by R. K. Shah, A. D. Kraus and D. Metzger), pp. 123–149. Hemisphere, New York (1990).
2. W. M. Kays and A. L. London, Heat transfer and flow friction characteristics of some compact heat-exchanger surfaces, Part I. Test system and procedure, *J. Heat Transfer* **72**, 1075–1085 (1950).
3. W. M. Kays, The basic heat transfer and flow friction characteristics of six compact high-performance heat transfer surfaces, *J. Engng Power* January, 27–34 (1960).
4. D. C. Briggs and A. L. London, The heat transfer and flow friction characteristics of five offset rectangular duct and six plain triangular plate-fin heat transfer surfaces. In *International Developments in Heat Transfer*, pp. 122–134. ASME, New York (1961).
5. A. L. London and R. K. Shah, Offset rectangular plate-fin surfaces—heat transfer and flow friction characteristics. *Trans. J. ASME* **218**–228 (1968).
6. S. Mochizuki and Y. Yagi, Heat transfer and friction characteristics of strip fins, *Jap. Res.* **6**, 36–59 (1977).
7. S. Mochizuki, Y. Yagi and W. J. Yang, Transport phenomena in stacks of interrupted parallel-plate surfaces, *Expl Heat Transfer* **1**, 127–140 (1987).
8. E. M. Sparrow and A. Hajiloo, Measurements of heat transfer and pressure-drop for an array of staggered and continuous plate heat exchangers, *J. Heat Transfer* **102**, 426–432 (1980).
9. H. M. Joshi and R. L. Webb, Heat transfer and friction in the offset strip-fin heat exchanger. *Int. J. Heat Mass Transfer* **30**, 69–84 (1987).
10. A. R. Wieting, Empirical correlations for heat transfer and flow friction characteristics of rectangular offset-fin plate-fin heat exchangers, *Trans. ASME J. Heat Transfer* **97**, 488–490 (1975).
11. W. M. Kays and A. L. London, *Compact Heat Exchangers* (3rd Edn). McGraw-Hill, New York (1984).

12. J. M. Robertson, Boiling heat transfer with liquid nitrogen in brazed-aluminum plate-fin heat exchangers, *AIChE. Symp. Ser.* **189**, 151–164 (1979).
13. R. Brinkmann, S. Ramadhyani and F. P. Incropera, Enhancement of convective heat transfer from small heat sources to liquid coolants using strip fins, *Expl Heat Transfer* **1**, 315–330 (1987).
14. K. S. Hou, Thermal performance of offset strip fins under unsymmetrical heating condition for various fluids, Master's Thesis, California State University, CA (1988).
15. Y. N. Marr, Correlating data on heat transfer in plate-fin heat exchangers with short offset fins, *Thermal Engng* **37**(5), 249–252 (1990).
16. R. LeVasseur, Liquid cooled approaches for high density avionics, *Proceedings of IEEE/AIAA Tenth Digital Avionics Systems Conference*, pp. 147–152 (1991).
17. R. J. Philips, Forced-convection, liquid-cooled, microchannel heat sinks, TR-787, Massachusetts Institute of Technology, MA (1988).
18. R. K. Shah and A. L. London, *Laminar Flow Forced Convection in Ducts—a Source Book for Compact Heat Exchanger Analytical Data*. Academic Press, New York (1978).
19. S. Hu and K. E. Herold, Prandtl number effect on offset fin heat exchanger performance: predictive model for heat transfer and pressure drop, *Int. J. Heat Mass Transfer* **38**, 1043–1051 (1995).
20. S. Hu, Heat transfer and pressure drop of liquid cooled offset fin heat exchanger, PhD Dissertation, University of Maryland, MD (1993).
21. S. L. Kline, The purposes of uncertainty analysis, *J. Fluid Engng* **107**, 153–164 (1985).